Editors' Suggestion | Featured in Physics

Bend or Twist? What Plectonemes Reveal about the Mysterious Motility of *Spiroplasma*

Paul M. Ryan,[1,*] Joshua W. Shaevitz,[2] and Charles W. Wolgemuth[1,3,†]
[1]*Department of Physics, University of Arizona, Tucson, Arizona 85721, USA*
[2]*Joseph Henry Laboratories of Physics and Lewis-Sigler Institute for Integrative Genomics, Princeton University, Princeton, New Jersey 08544, USA*
[3]*Department of Molecular and Cellular Biology, University of Arizona, Tucson, Arizona 85721, USA*

(Received 22 February 2023; accepted 15 September 2023; published 24 October 2023)

Spiroplasma is a unique, helical bacterium that lacks a cell wall and swims using propagating helix hand inversions. These deformations are likely driven by a set of cytoskeletal filaments, but how remains perplexing. Here, we probe the underlying mechanism using a model where either twist or bend drive spiroplasma's chirality inversions. We show that *Spiroplasma* should wrap into plectonemes at different values of the length and external viscosity, depending on the mechanism. Then, by experimentally measuring the bending modulus of *Spiroplasma* and if and when plectonemes form, we show that *Spiroplasma*'s helix hand inversions are likely driven by bending.

DOI: 10.1103/PhysRevLett.131.178401

A static helix is defined by two parameters: the radius of curvature R and pitch P, or the curvature $\kappa_0 = R/\left(R^2 + (P/2\pi)^2\right)$ and torsion $\tau_0 = (P/2\pi)/\left(R^2 + (P/2\pi)^2\right)$. The local shape of a rodlike object (i.e., an object that is long in one dimension and thin in the other two) is described by a strain vector $\mathbf{\Omega}$, which has three independent components defining two perpendicular bends (or curvatures) and the twist per length about the long axis. Consequently, a helical rod of length L can be described in two different ways, one involving twist and bend with $\Omega_1 = \kappa_0$, $\Omega_2 = 0$, and $\Omega_3 = \tau_0$ [Fig. 1(a)], and the other that only uses bending, with $\Omega_1 = \kappa_0 \cos(2\pi s/\tau_0)$, $\Omega_2 = \kappa_0 \sin(2\pi s/\tau_0)$, $\Omega_3 = 0$, and s the length measured along the rod's centerline [Fig. 1(b)].

While both of these helices look the same, it may not take the same amount of work to form them. For a linearly elastic rod of circular cross section and equilibrium curvatures κ_1 and κ_2 and torsion τ, the moment required to deform the rod away from this shape is

$$\mathbf{M} = A[(\Omega_1 - \kappa_1)\mathbf{e}_1 + (\Omega_2 - \kappa_2)\mathbf{e}_2] + C(\Omega_3 - \tau)\mathbf{e}_3, \quad (1)$$

where the filament's centerline is parametrized using a vector $\mathbf{r}(s)$, and we have defined an orthonormal triad at each point $(\mathbf{e}_1, \mathbf{e}_2, \mathbf{e}_3)$, such that $\mathbf{e}_3 = \partial\mathbf{r}/\partial s$ is the tangent vector, and $\mathbf{e}_1$ and $\mathbf{e}_2$ lie in the plane perpendicular to the tangent. The bending modulus A defines the moment required to impose a given curvature, while the twisting modulus C is the material stiffness with respect to twisting motions. In general, $C \neq A$ [6], and twist enters the dynamic equations for the centerline in a different way than preferred curvature (e.g., see Ref. [7]). Therefore, we expect twist-driven dynamics to differ from those driven by bend. In this Letter, we use this distinction to probe the

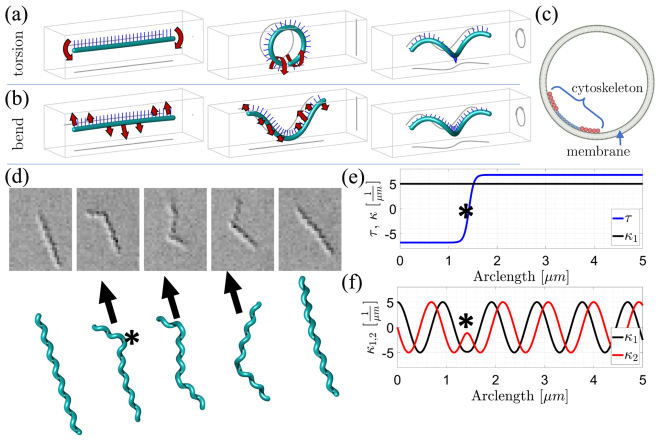

FIG. 1. (a) To create a helix by twisting, a straight rod can first be bent into a planar curve with constant radius κ_0^{-1} and then twisted about its length with twist density τ_0. (b) To create one by bending, first bend the rod into a planar, sinusoidal wave, and then bend it along the perpendicular direction into another sinusoidal wave, 90° out of phase from the first wave. In (a) and (b) the red arrows show the bend and twist directions, and the blue lines point along $\mathbf{e}_2$. Note that the resulting $\mathbf{e}_2$ vectors do not point in the same direction in (a) and (b). (c) Cross section of *Spiroplasma* showing the internal cytoskeletal ribbon with (red) Fibril protein filaments and (blue) SpMreB filaments, as described in [1]. (d) Experiment (top) and bend-model simulation (bottom) of a swimming *Spiroplasma* at low viscosity (see Supplemental Material movie S1 [2]). The solid arrow indicates swimming direction, the $*$ represents the junction ("kink") between RH and LH chirality, and time progresses left to right in the figure. The preferred torsion, τ, and curvatures, $\kappa_{1,2}$ as a function of arclength for a *Spiroplasma* with a chirality inversion versus length for the torsion-based (e) and curvature-based (f) models where $*$ indicates the location of the kink.

perplexing motility mechanism of the unique bacterium *Spiroplasma*.

While many bacteria swim by rotating external helical flagella [8], *Spiroplasma* swims by propagating periodic inversions of its chirality [9–11]. *Spiroplasma* are predominantly seen in electron microscopy as right-handed (RH) helices [11,12]. To swim, the handedness of the cell body switches to left handed (LH) starting at one end [11]. This helix hand inversion grows from that end, propagating down to the opposite end at speed $v_k \sim 10$ μm/s [Fig. 1(d), [11]] The location of the chirality change is identifiable as a translating kink in the cell body [10]. After a time t_k, the first end reverts to its original RH conformation, and this change in helicity propagates to the far end with the same velocity as the first kink.

Not only is the swimming mechanism of *Spiroplasma* unique, so is its structure. The cells are wall-less, lacking the elastic peptidoglycan layer that defines the shape of most bacteria [13,14]. *Spiroplasma*, instead, only has a liquidlike lipid membrane separating the inside of the cell from the outside. The helical shape and dynamic change in chirality is attributed to an internal set of cytoskeletal filaments [1,13,15,16] [Fig. 1(c)]. Although recent work has shed light on the interaction between *Spiroplasma*'s cytoskeleton and membrane, how the cytoskeletal filaments drive the periodic helix hand inversions has only been conjectured, with little evidence to support any given idea [10,17–19].

Here we ask the simple question: Do these cytoskeletal filaments induce helicity flipping through a bend or twist mechanism? While previous researchers have successfully used torsion-based models to reproduce the kinematics of *Spiroplasma*'s motility in low viscosity fluids [20–22], it is unclear whether these models are a faithful representation of the actual mechanics.

To investigate the mechanics of *Spiroplasma*, we treat the bacterium as an elastic filamentary object with circular cross section of radius a. At low Reynolds number, a filament's elastic restoring forces $\mathbf{F}$ are balanced by the viscous drag per length from the fluid, $\mathbf{f}_d = \partial\mathbf{F}/\partial s$ [23], where the drag force is approximately proportional to the local velocity of the filament and also linearly dependent on the fluid viscosity η. Moment balance along the filament defines the restoring forces [24],

$$\frac{\partial \mathbf{M}}{\partial s} = -\mathbf{e}_3 \times \mathbf{F} + \zeta_r \omega_3 \mathbf{e}_e, \tag{2}$$

with $\zeta_r = 4\pi\eta a^2$ the rotational drag coefficient and the moment as given in Eq. (1). These equations give dynamics where the local velocity of the filament is related to second derivatives of the curvatures but only first derivatives of the twist. We hypothesize that these differences in dynamics will lead to different behaviors depending on the external viscosity.

To model the case where chirality flipping is induced by a twisting mechanism, we define the preferred curvatures for *Spiroplasma* to be $\kappa_1 = \kappa_0 = 5.0\ \mu\text{m}^{-1}$ and $\kappa_2 = 0$ [11]. We then drive the helicity dynamics using

$$\tau(s,t) = \tau_0 \mathcal{F}(s,t), \tag{3}$$

where $\tau_0 = 6.8\ \mu\text{m}^{-1}$ and the function $\mathcal{F}$ is defined as

$$\begin{aligned}\mathcal{F}(s,t) = 1 &+ \tanh\left(\beta[s + v_k(t_1 - t)]\right) \\ &- \tanh\left(\beta[s + v_k(t_1 + t_k - t)]\right).\end{aligned} \tag{4}$$

This definition flips the torsion between $\pm\tau_0$, with β controlling the slope of the hyperbolic tangent transition and t_1 the time at which the first helicity change occurs [Fig. 1(e)]. We also use $t_k = 0.25$ s, and $\beta = 70$ to match experimental values observed for *Spiroplasma melliferum* [11]. This model for the dynamics is similar to what previous groups have used [20–22].

On the other hand, *Spiroplasma*'s shape could be generated by bending. For this case, we set $\tau = 0$ and use sinusoidally varying preferred curvatures [Fig. 1(f)],

$$\begin{aligned}\kappa_1(s,t) &= \kappa_0 \sin\left(\int_0^s ds' \tau_0 \mathcal{F}(s',t)\right), \\ \kappa_2(s,t) &= \kappa_0 \cos\left(\int_0^s ds' \tau_0 \mathcal{F}(s',t)\right),\end{aligned} \tag{5}$$

where $\kappa_0 = 5.0$ and $\mathcal{F}$ is defined the same as in Eq. (4).

From a purely kinematic viewpoint, these two mechanisms are indistinguishable. To determine whether changing the external viscosity leads to different dynamical behaviors, we simulated the dynamics of *Spiroplasma* using the regularized Stokeslet approach first published in [25,26], combined with a finite volume approach for computing the elastic restoring forces [2,27]. Briefly, we define the moment as in Eq. (1) and use the finite volume approach to compute the force per length from Eq. (2). If we apply these forces and moments at the centerline using delta functions, the Stokes equation for the fluid is $-\nabla p + \eta\nabla^2\mathbf{u} + [\mathbf{F} + \frac{1}{2}\boldsymbol{\nabla} \times \mathbf{M}]\delta(\mathbf{x} - \mathbf{x}_0) = 0$, where p is pressure, $\mathbf{x}$ is a point in the fluid, and $\mathbf{x}_0$ is a centerline location where the forces are applied. To solve this equation computationally, we regularize (spread) the delta function in the same fashion as [25,26] using a spherically symmetric cutoff function, $\phi_\epsilon(r)$, where

$$\phi_\epsilon(r) = \frac{15\epsilon^4}{8\pi(r^2 + \epsilon^2)^{7/2}}, \tag{6}$$

with $r = |\mathbf{x} - \mathbf{x}_0|$ and ϵ controlling the degree to which this function is spread. Note that $\phi_\epsilon(\mathbf{x})$ becomes a delta function as $\epsilon \to 0$. This method does not explicitly define the cell's width. Therefore, to determine the effective cell

body radius produced by a given ϵ, we simulated an initially straight filament with zero twist. One end of the filament was then clamped and rotated parallel to the long axis at a rate ω_3 that is below the critical buckling frequency, as in [28,29]. We then measure the torque $C\Omega_3$ that is necessary to achieve a specific rotational frequency. The effective radius a_e is then determined as $C\Omega_3 = \zeta_r \omega_3 L = 4\pi\eta a_e^2 \omega_3 L$, from which we find that $a_e \approx 0.710\epsilon$.

To complete the mechanical description of *Spiroplasma*, we also need to define the bending and twisting moduli in Eq. (1), which have not been previously measured. To do this, we used an optical trapping system to pull on *S. melliferum* wild type *A*77 and measured the force required to stretch the cell body a distance Δx. A schematic of our optical trapping system is shown in Fig. 2(a), with further details on our experimental procedure given in the Supplemental Material [2]. Our experimental protocol included forces that both extended and compressed the helical cell body along its axis. However, we found that fitting the data to extract the value of the bending modulus was most sensitive to the extensional region of the data. Therefore, we fit the experimental data to the force extension curve for a pure axial stretching force generated using a range of values for the ratio C/A (see the Supplemental Material for details [2]). We found that the data were well fit for values of $0.5A \leq C \leq A$, while when $C < 0.5A$ the fits were less good, did not always converge, and gave unreasonable values for the cell length (see the Supplemental Material and Fig. S3). This result suggests that $0.5 \leq C/A \leq 1$, since most materials cannot have a value greater than 1 [30]. Fitting the data then gave a range $A = 0.14 \pm 0.03$ pN μm^2 for $C/A = 1$, and $A = 0.17 \pm 0.02$ pN μm^2 for $C/A = 0.5$. Combining these results, we find $A = 0.15 \pm 0.04$ pN μm^2.

Using the measured bending modulus, we ran simulations of the bend- and torsion-based models over a range of viscosities from 1.0 to 20.0 cP. The length of *Spiroplasma* was discretized using a grid spacing $\Delta s = 0.075$ μm, and we set $\epsilon = 1.68\Delta s$ in order to ensure that the effective radius was within 5% of 0.09 μm, the value determined by electron microscopy studies [31]. For low viscosities (∼1 cP) and lengths of less than 7 μm, the bend- and torsion-based models were nearly identical and accurately reproduced the swimming dynamics of *Spiroplasma*, as shown in Fig. 1(d). However, at larger viscosities and/or longer lengths, the two models deviate. The agreement between the two mechanisms at low viscosity and/or short lengths is due to the fact that both mechanisms drive the motion by equivalent preferred kinematics. We can define an elastic relaxation time $T_{\rm el} \propto \eta L^4/A$. When this time is fast compared with the forcing timescale ($\sim L/v_k$), both mechanisms closely follow the preferred kinematics. However, when the elastic timescale is comparable to or slower than the forcing timescale, the two mechanisms will deviate from the defined kinematics and potentially from each other. We find that for a given length L and kink speed v_k, there is a viscosity above which the simulations predict that a swimming *Spiroplasma* folds over onto itself and wraps into a plectoneme, as shown in Fig. 3. In our simulations, we define a plectoneme when any node at arclength s along the cell body comes into contact with another node between the arclengths $2\pi P \leq s' \leq L - 2\pi P$. This definition excludes self-contact with the edge nodes, which we do in order to compare to the experiments described later, where contact involving the cell extrema will not alter the bacterium's motion enough to be observable in one 10 ms frame. This viscosity at which a plectoneme is observed is lower for the torsion-based model than for the bend-based model. We speculate that plectoneme formation is due to a buildup in twist as the kink propagates down the length of the cell, since the cell has to rotate about its helical axes in order to alternate handedness. If this hypothesis is correct, we expect from dimensional analysis and by analogy with the dynamics for twirling a straight filament [28] that the critical rotational frequency at which the cell buckles and potentially wraps around itself is given by $\omega_c \propto A/\zeta_r L^2$, where the constant of proportionality can be different for the two mechanisms. This frequency should also be related to the rate that twist is injected into the cell by the traveling kink, which should be proportional to $2\tau_0 v_k$, since the traveling kink flips the torsion between $\pm\tau_0$. Therefore, we expect the onset of plectoneme formation to scale like $L^2 \propto 1/\eta v_k$. This result implies there is a critical length at which plectonemes begin to form that is inversely proportional to ηv_k. Indeed, we find that the bend-based model begins to form plectonemes at longer lengths than what is predicted by the torsion-based model (Fig. 4).

To determine whether these results were informative about the mechanism of *Spiroplasma* motility, we used differential interference contrast microscopy to observe

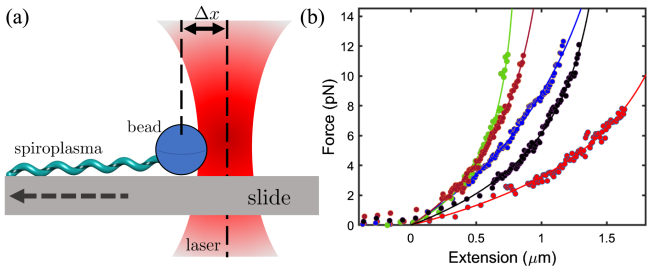

FIG. 2. (a) Schematic of the optical trapping setup. A *Spiroplasma* (green) is immobilized at one end by attachment to a glass cover slip (slide). A spherical bead (blue) trapped in an infrared laser (red) is attached to the *Spiroplasma*'s free end. The stage is then moved slowly so that the bacterium is stretched. The distance between laser axis and bead center, Δx, is measured to find the force. (b) Representative force vs extension curves with the best fit to the curve predicted for stretching an elastic helix, from which we find an average bending modulus $A = 0.15 \pm 0.04$ pN μm^2.

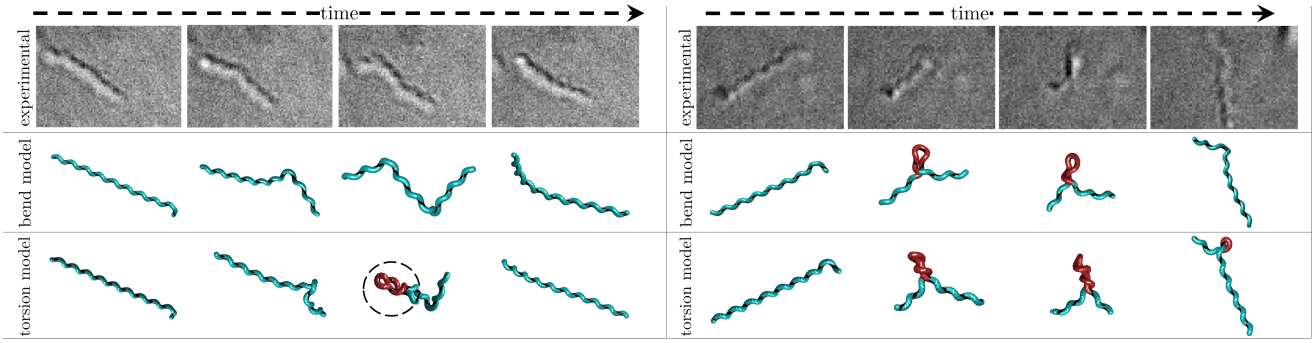

FIG. 3. Upper left: a *Spiroplasma* cell of length $L = 5.56$ μm swims through fluid with viscosity $\eta = 5.9$ cP exhibiting a measured kink speed, $v_k = 10.0$ μm/s [movies S2(a), S2(b), and S2(c) in the Supplemental Material [2]]. This bacterium never forms a plectoneme. Using the same parameters, the bend-based model's dynamics (middle left panels) agree well with experiment, while the torsion-based model (lower left panels) forms a plectoneme. Upper right: *Spiroplasma* length $L = 4.76$ μm swimming in fluid with $\eta = 10$ cP [movies S3(a), S3(b), and S3(c) [2]]. As a kink propagates along the cell ($v_k = 11.5$ μm/s), a plectoneme forms. Results of the bend (middle right panels) and torsion (lower left panels) model simulations with the same parameters. Plectonemic regions in the simulations are highlighted in red whereas the circled area is a plectoneme incorrectly predicted by the torsion-based model.

Spiroplasma swimming as a function of viscosity. We cultured *S. melliferum* and performed motility assays, following the procedure described in [11]. We varied the viscosity between 4 and 12 cP, in increments of ∼2 cP, using Ficoll®, which maintains the Newtonian fluid characteristics of the medium [32]. The viscosities of the media were measured directly from the mean squared displacement

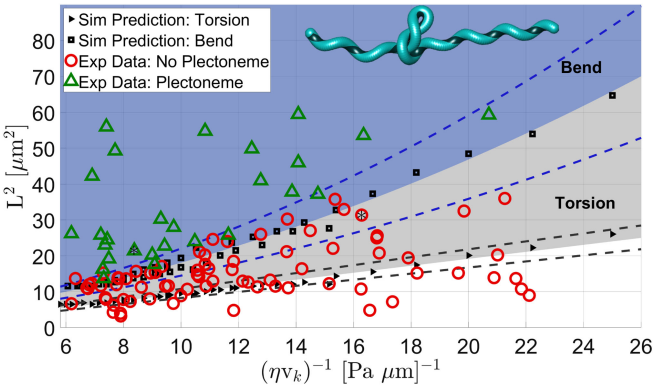

FIG. 4. Plectoneme formation as a function of length, viscosity, and kink speed. While the bend- and torsion-based models both predict that the length when plectonemes form depends on $1/\eta v_k$, the torsion-based model (black triangles) predicts plectonemes at shorter lengths than the bend-based model (black squares). Experimental observations found where in the L^2 vs $1/\eta v_k$ phase-space plectonemes occurred (green triangles) or did not occur (red circles). This experimentally determined plectoneme-forming region agrees well with that predicted by the bend-based model (blue-colored region), while the torsion-based model substantially overestimates the area of this region, with the gray coloring denoting where only the torsion-based model predicted plectonemes. The dashed blue (gray) lines indicate the variability in the onset of plectonemes when varying the bend modulus from $A = 0.14$–0.20 pN μm^2 for the bend (torsion) modalities while keeping the bend and twist moduli equal. The "*" indicates the experimental data points shown in Fig. 3.

(MSD) of suspended polystyrene beads, using custom written MATLAB code to compute the MSD in two dimensions (see the Supplemental Material). At low viscosities, we observed motility like what has been described previously [9–11] [Fig. 1(d)]. At higher viscosities, though, we observed many *Spiroplasma* undergoing altered motility in which the cell body formed plectonemes (Fig. 3). As shown in Fig. 3, we found parameters where the torsion-based model would predict plectonemes which were not observed for cells with similar parameters in experiments and in the bend-based model. Furthermore, in a parameter region where plectonemes were observed experimentally, the torsion-based model sometimes predicted persistent plectonemes that were not observed experimentally (see Fig. 3, right panels).

To compare to our modeling, we measured the length, kink speed, and viscosity on a total of 1100 individual propagating kinks across 104 individual *Spiroplasma* and recorded whether or not the bacterium formed a plectoneme. In these experiments, we found that the average kink velocities across all *Spiroplasma* were 11.65 ± 1.86 μm/s with no significant variation between viscosities, similar to what has been reported previously [11,33]. The results for the length as a function of $1/\eta v_k$ were then plotted on top of the predicted behavior from the two models, as shown in Fig. 4. The parameter region for where plectonemes were observed agrees surprisingly well with the predictions from the bend-based model, while the torsion-based model incorrectly predicts that plectonemes should form at significantly shorter lengths or lower viscosities than what is experimentally observed.

Here, we have leveraged a potentially underappreciated aspect of filament physics, that helices created by bend are not dynamically equivalent to those created by twist, in order to examine the biomechanics and motility of *Spiroplasma*. To begin to elucidate the mysterious motility

mechanism of this unique bacterium, we probed this dynamic difference in the context of helix hand inversions at low Reynolds number. Our results provided two n ew pieces of information about the biomechanics of *Spiroplasma*. First, we measured the bending modulus of the cell and found $A = 0.15 \pm 0.04$ pN μm^2, about 3 times stiffer than actin [34], and also put limits on the value of the twist modulus that $C > 0.5A$. Second, we showed that for the basic kinematic behavior of *Spiroplasma* swimming, the bend-based mechanism better predicts when *Spiroplasma* forms plectonemes as the viscosity is increased, thereby suggesting that this mechanism dominates over a twist-based one. While the specific details for how the spiroplasmal cytoskeleton produces motility remain elusive, our findings limit the possible underlying molecular mechanics and provide clues as to how *Spiroplasma*'s cytoskeletal filaments drive swimming. Indeed, our results may be consistent with a recent study that hypothesized a potential mechanism where SpMreB attaching and detaching from the membrane drives local curvature in the membrane and cell body [19]. Our results may also help explain other recent studies where reconstitution of the *Spiroplasma* cytoskeleton in a nonmotile bacterium confers motility to an otherwise inert cell [16,35].

This research was partially funded by the National Institutes of Health Grant No. T32 GM132008 and NSF Grant No. 2217661.

*paulryan@arizona.edu
†wolg@arizona.edu

[1] J. Kurner, A. S. Frangakis, and W. Baumeister, Science **307**, 436 (2005).
[2] See Supplemental Material at http://link.aps.org/supplemental/10.1103/PhysRevLett.131.178401 for a detailed description of the experimental, computational, and data analysis methods, which includes Refs. [3–5].
[3] R. Cortez, L. Fauci, and A. Medovikov, Phys. Fluids **17**, 031504 (2005).
[4] V. A. Harmandaris and M. Deserno, J. Chem. Phys. **125**, 204905 (2006).
[5] M. D. Koch and J. W. Shaevitz, Methods Mol. Biol. **1486**, 3 (2017).
[6] S. Wolff-Vorbeck, M. Langer, O. Speck, T. Speck, and P. Dondl, Sci. Rep. **9**, 17182 (2019).
[7] W. Kan and C. W. Wolgemuth, Biophys. J. **93**, 54 (2007).
[8] N. Wadhwa and H. C. Berg, Nat. Rev. Microbiol. **20**, 161 (2022).
[9] J. Roth, M. D. Koch, and A. Rohrbach, Biophys. J. **114**, 1955 (2022).
[10] R. Gilad, A. Porat, and S. Trachtenberg, Mol. Microbiol. **47**, 657 (2003).
[11] J. W. Shaevitz, J. Y. Lee, and D. A. Fletcher, Cell **122**, 941 (2005).
[12] E. Ammar, D. Fulton, X. Bai, T. Meulia, and S. Hogenhout, Arch. Microbiol. **181**, 97 (2004).
[13] S. Trachtenberg, J. Struct. Biol. **124**, 244 (1998).
[14] A. Typas, M. Banzhaf, C. Gross, and W. Vollmer, Nat. Rev. Microbiol. **10**, 123 (2012).
[15] Y. Sasajima, T. Kato, T. Miyata, A. Kawamoto, K. Namba, and M. Miyata, Front. Microbiol. **13**, 1004601 (2022).
[16] H. Kiyama, S. Kakizawa, Y. Sasajima, Y. O. Tahara, and M. Miyata, Sci. Adv. **8**, abo7490 (2022).
[17] C. W. Wolgemuth, O. Igoshin, and G. Oster, Biophys. J. **85**, 828 (2003).
[18] S. Harne, P. Gayathri, and L. Beven, Front. Microbiol. **11**, 589279 (2020).
[19] Y. Sasajima and M. Miyata, Front. Microbiol. **12**, 2198 (2021).
[20] H. Wada and R. R. Netz, Phys. Rev. Lett. **99**, 108102 (2007).
[21] C. Esparza López and E. Lauga, Phys. Rev. Fluids **5**, 093102 (2020).
[22] J. Yang, C. W. Wolgemuth, and G. Huber, Phys. Rev. Lett. **102**, 218102 (2009).
[23] E. Lauga and T. R. Powers, Rep. Prog. Phys. **72**, 096601 (2009).
[24] E. M. Strawbridge and C. W. Wolgemuth, Phys. Rev. E **86**, 031904 (2012).
[25] R. Cortez, SIAM J. Sci. Comput. **23**, 1204 (2001).
[26] S. D. Olson, S. Lim, and R. Cortez, J. Comput. Phys. **238**, 169 (2013).
[27] P. M. Ryan and C. W. Wolgemuth, J. Comput. Phys. **466**, 111375 (2022).
[28] C. W. Wolgemuth, T. R. Powers, and R. E. Goldstein, Phys. Rev. Lett. **84**, 1623–6 (2000).
[29] P. M. Ryan and C. W. Wolgemuth, Phys. Rev. Fluids **7**, 113101 (2022).
[30] A. E. H. Love, *A Treatise on the Mathematical Theory of Elasticity*, 4th ed. (Dover Publications, New York, 1944).
[31] S. Trachtenberg, P. Schuck, T. M. Phillips, S. B. Andrews, and R. D. Leapman, PLoS One **9**, e87921 (2014).
[32] X. Chen and H. C. Berg, Biophys. J. **78**, 1036 (2000).
[33] J. Boudet, M. Mathelie-Guinlet, A. Vilquin, J. Douliez, L. Beven, and H. Kellay, Sci. Rep. **8**, 17138 (2018).
[34] F. Gittes, B. Mickey, J. Nettleton, and J. Howard, J. Cell Biol. **120**, 923 (1993).
[35] C. Lartigue, B. Lambert, F. Rideau, Y. Dahan, M. Decossas, M. Hillion, J.-P. Douliez, J. Hardouin, O. Lambert, A. Blanchard, and L. Beven, Nat. Commun. **13**, 6930 (2022).